
# Green PE

# WP3: ADVANCED POWER ELECTRONICS FOR RENEWABLE ENERGIES TECHNICAL REPORT

Interreg
Baltic Sea Region

EUROPEAN UNION
EUROPEAN REGIONAL DEVELOPMENT FUND

**Authors:**

*Steffen Chemnitz, Kiel University*
*Mariusz Sochacki, Warsaw University of Technology*

**Published in February 2019**

**Lead Partner:**

University of Southern Denmark
Alsion 2
6400 Sønderborg
Denmark

Contact: Horst-Günter Rubahn
rubahn@mci.sdu.dk
Phone: +45 6011 3517

www.sdu.dk/en/om_sdu/institutter_centre/mci_mads_clausen

www.balticgreenpower.eu

TABLE OF CONTENT

# 1.Introduction

One main part of the Green Power Electronics (Green PE) project was to demonstrate the potential, feasibility and relevance of advanced power electronics (PE) based solutions in the application fields of renewable energies, e-mobility and smart houses.

This document refers to the pilot within the application field of renewable energies that consists of two pilot demonstrators:

- Pilot demonstrator A1: A SiC-based DC – AC inverter in Kiel, Germany
- Pilot demonstrator A2: A GaN-based inverter in Warsaw, Poland

The aim of this technical report is to present the activities including results being done to demonstrate new solutions for applications of advanced power electronics within the renewable energy sector.

The main target groups of this demonstrator are power electronic companies with renewable energy business, especially in the field of advanced power converters, as well as research institutes and universities.

# 2. A SiC-based DC – AC inverter in Kiel, Germany

## 2.1. Introduction

All modern societies are faced to the challenge of a carbon dioxide neutral electrical energy supply, which includes (besides of many other developments) the demand for much more power electronics and an efficient power conversion in the future.
This pilot within the Green PE project covers at one hand the idea to implement three innovative concepts (wide bandgap semiconductors for a better efficiency, zero voltage switching for less conversion losses, 3-level topology for cheaper devices) into a converter for solar applications. In addition, this demonstrator is then presented at exhibitions, fairs and conferences to discuss the innovations with possible customers and manufacturers.
Main goals of these pilot activities are:

- to identify the potential of the innovations in terms of a possible realization,
- to identify prospective applications and novel markets due to the innovations,
- to intensify existing and possible future collaborations,
- to identify and investigate existing market entry barriers, and
- to discuss technology transfer from research institutes to companies.

## 2.2. Topology and ZVS Control

The DC-AC converter within this demonstrator is a single phase non-isolated power inverter and implements a 3-level-topology, where the positive and negative half wave of the output voltage is delivered by designated buck converters each. These converters limit – as the major reason – the maximum output voltage for the semiconductor devices and reduces therefore the costs of it. Fig. 2.1 shows the topology.

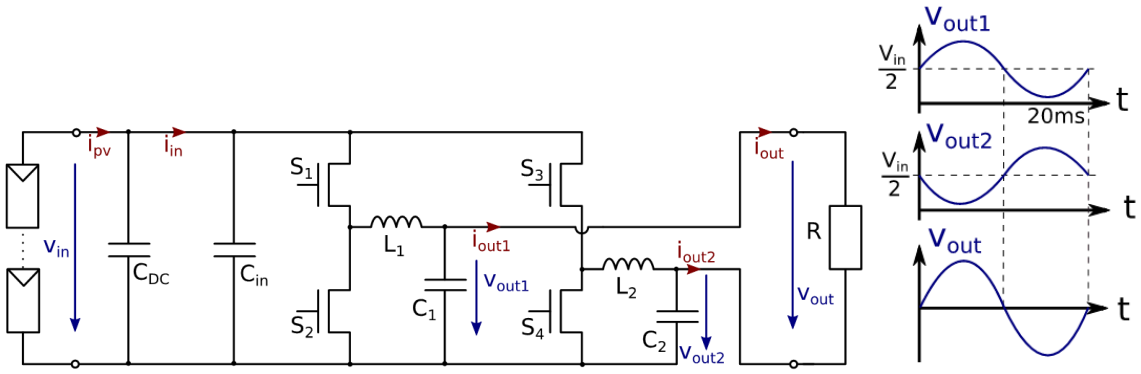


*Figure 2.1: Schematics of the topology for the DC-AC converter.*
*Source: Green PE project.*

Both buck converters are controlled by a 180° phase shift differential and deliver a sinusoidal 50 Hz output voltage, as depicted in Fig. 2.1 with output voltage on the right.
As a second feature, the converter uses a zero voltage switching (ZVS) concept to minimize the switching losses and to increase the conversion efficiency.

To take the full advantage of wide bandgap semiconductor devices (and here commercially available SiC devices have been used), the switching frequency is substantially increased to up to 400 kHz, compared to traditional converter concepts. This leads to the additional opportunity of using small passive components, as the inductor and capacitor dimensions scale inversely with the frequency.
But on the other hand, this concept requires a much more sophisticated control. In detail:

- A ZVS through modulation of switching frequency, duty cycle and time delay,
- output level dependence on input and output voltage and output current, and
- up to 220,000 operating points and 1800 calculations per period.

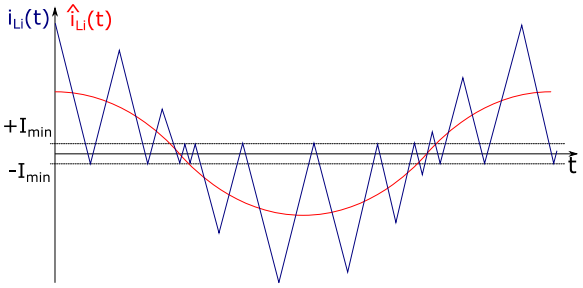


$$f_{OPT}(t) = \begin{cases} \dfrac{V_{in}V_{out} - {V_{out}}^2}{2\,V_{in}\,L\,(I_{min} + I_L(t))} & I_L(t) \geq 0 \\ \dfrac{V_{in}V_{out} - {V_{out}}^2}{2\,V_{in}\,L\,(I_{min} - I_L(t))} & I_L(t) < 0 \end{cases}$$

*Figure 2.2: Soft switching concept with its state depending switching frequency $f_{opt}(t)$.*
*Source: Green PE project.*

This so-called "soft switching" is achieved on both buck converters individually and results in a variable, optimal switching frequency [see 1], depending on the actual inductor current and input/output voltages, according to Fig. 2.2:

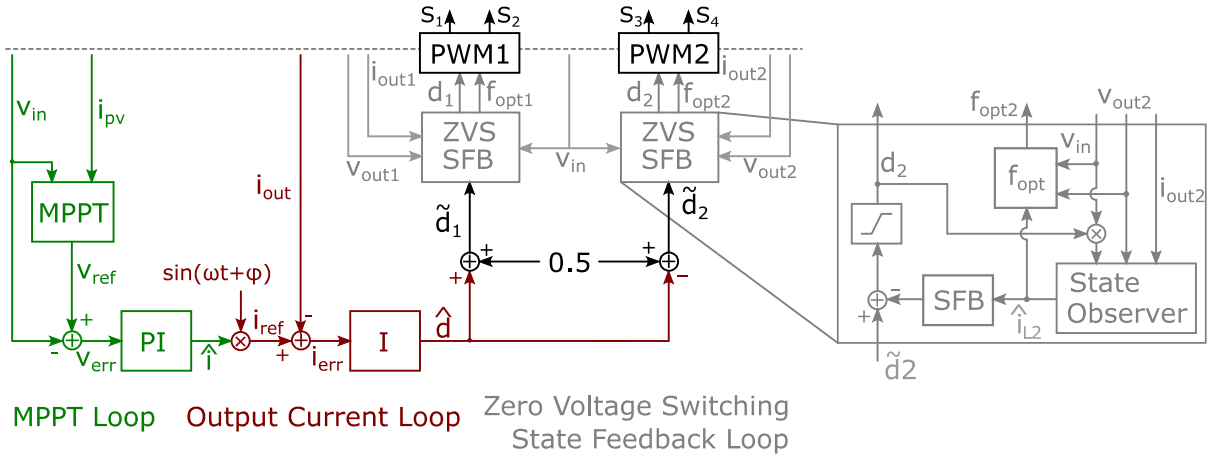


*Figure 2.3: Soft switching concept with its state depending switching frequency $f_{opt}(t)$.*
*Source: Green PE project.*

Transferring the described concept to an efficient control setup, some prerequisites become essential:

- The substantial losses in switches and capacitors are minimized
- SiC switches are turned on when $V_{DS} < 0$ and $I_D < 0$
- $I_{L,i}(t)$ is determined using a state observer
- State feedback control determines the duty cycle, dead time and frequency.

This leads to a control scheme as developed and used for the demonstrator and is shown in Fig. 2.3:

The right hand side of Fig. 2.3 shows the integrated control scheme for ZVS with a state observer circuitry and on the left hand side the integration of the Maximum Power Point Tracker (MPPT) is displayed, which provides the ZVS with a feedback signal to adjust the output current to the maximum input power, provided by the input solar panels in this application. The next section explains its function and limitation.

## 2.3. MPP Tracking for photovoltaic applications

The MPP Tracker is a need for applications, where energy is converted from a limited source in terms of power. Therefore, the converter is equipped with an additional feedback loop, adjusting the delivered output to the input power, provided by the solar panels. Fig. 2.4 shows this scheme for a set of solar irradiations.

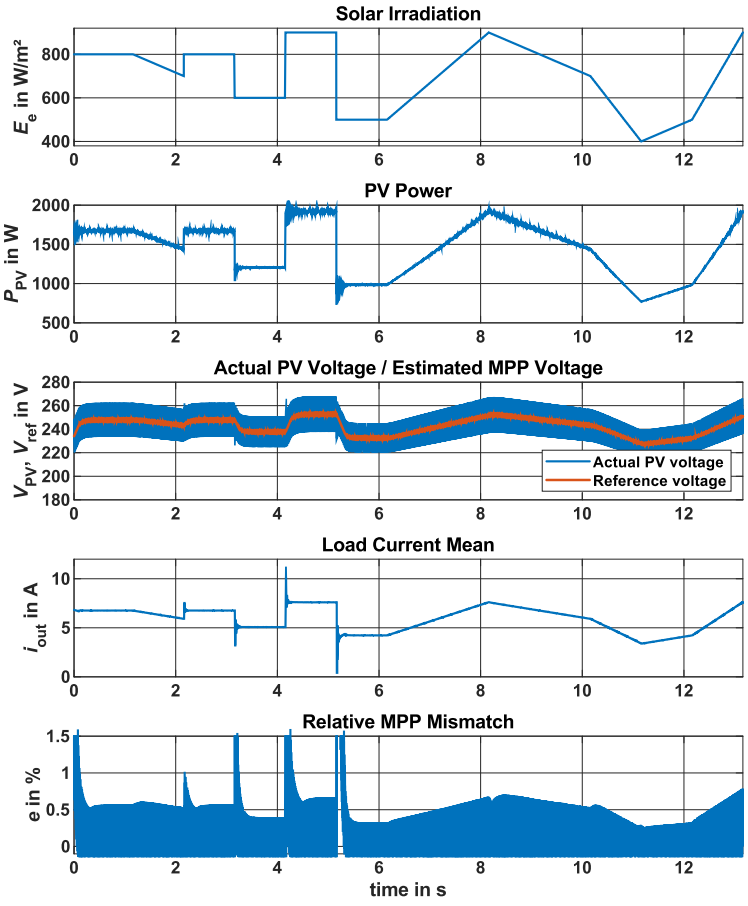


*Figure 2.4: Resulting, relative MPPT mismatch for the converter current, voltage and power for different solar irradiation scenarios. Source: Green PE project.*

Comparison and simulation of different algorithms suggest usage of the Perturb and Observe algorithm:

- Simple and robust implementation
- MPPT mismatch <0.6% for steady state and ramps≤ $300\ {}^{\mathrm{W}}/_{\mathrm{m^2 s}}$
- Minimum MPPT mismatch due to 100 Hz ripple and $C_{DC}$ buffer
- Small voltage step size and high MPPT frequency (≈15 kHz) avoid additional steady state ripple

An average mismatch of this control is below 0.5% and is a well-balanced trade-off in terms of efficiency and complexity, as the unused power input introduced by the MPPT does not contribute to the internal losses and an internal thermal heat dissipation. The effective tracking is demonstrated later in the lab test section.

## 2.4. Device Specification

The development of the converter involved two major innovations for an increased conversion efficiency. First, the use of wide bandgap semiconductor devices and secondly, the implementation of Zero-Voltage-Switching. Both results in an overall efficiency of 97 percent and will be further improved by an ongoing optimization. Simulations demonstrated that the conversion efficiency ranges between 99 and 99.5 % for loads above 10% full power.

*Figure 2.5: Picture of the realized single phase DC/DC converter with the control board, the connectors, the internal flyback and buck converters on the right and the passive components on the left hand.*
*Source: Green PE project.*

This makes the device very competitive to applications especially at light loads, where the photovoltaic application with its various irradiation conditions is an excellent example of it.

Input /output characteristics and main parts of the converter:

- Input voltage: 400 $V_{DC}$
- Output voltage: 230 $V_{AC}$
- Max power: 2.5 kW
- SiC MOSFET (<400 kHz sw. freq.)
- 150 ps switching resolution (HRPWM)
- FlyBack System Power
- FlyBuck Gate Driver Power
- Infineon XMC ARM Cortex M4
- C2000 ControlCard interface
- 14bit, 2.5MSPS, 84dB SNR ADCs

The innovation of this converter topology has not only its efficiency as a single advantage, it goes along with a significant increase of the power to volume ratio, which is approx. 2.5kW/L and results in a very compact design of the converter.

Furthermore, and probably most attractive for prospective customers, is the effect, that a high efficiency implies low internal losses as shown in Fig. 2.6.

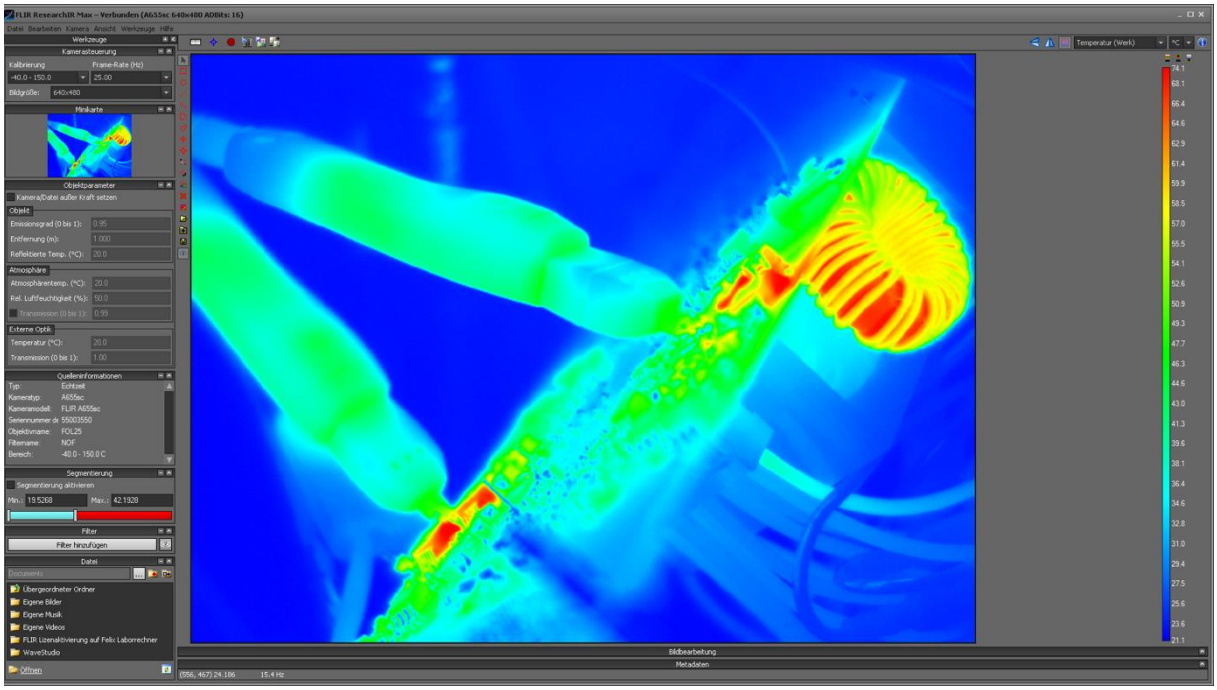

*Figure 2.6: Picture of the thermal analysis of the control board.*
*Source: Green PE project*

For this reason, the realized device as depicted in Fig. 2.5 does not contain and does not require an active cooling nor a radiator block or any moving parts for heat dissipation, as the losses are reduced to a minimum.

This is a very positive side effect of the internal efficiency and opens new applications, where an implementation of active cooling and rotating parts are complicated, such as harsh environments. Section 2.6 discusses this in detail.

## 2.5. Laboratory performance and influence on applications

Testing and implementation:

- The tests are conducted using a setup with a passive resistive load and demonstrate at the present development stage the feasibility of the control concept
- Output voltages and current are measured

In the upper graph of Fig. 2.7 are both buck converter output voltages displayed. In combination, they result in the final output. Voltage and current (displayed in green and red) are here in phase, as a resistive load has been used at the output terminals.

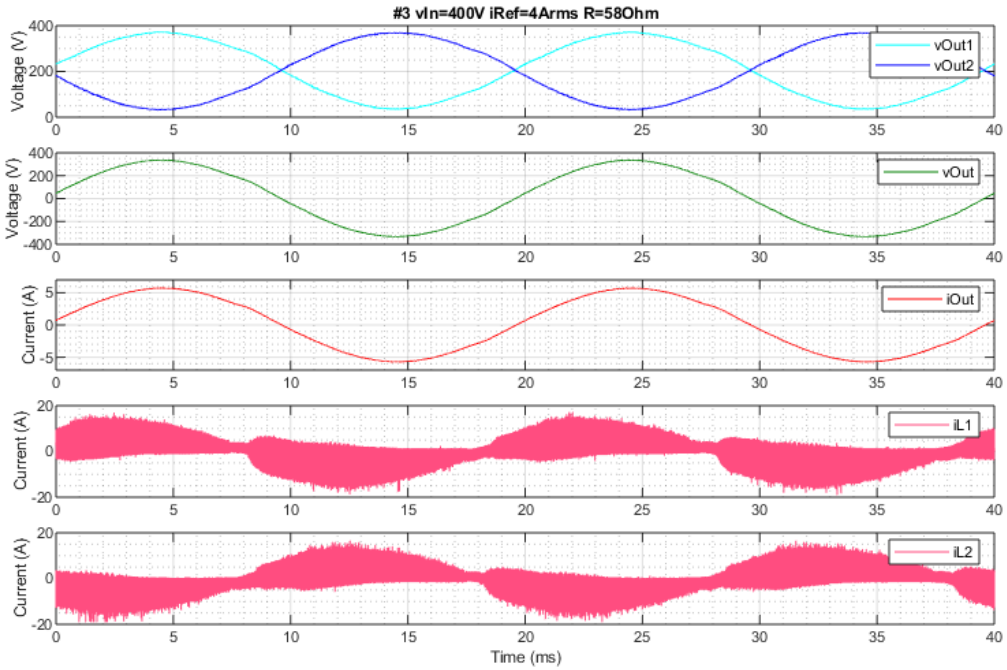


*Figure 2.7: Resulting, relative MPPT mismatch for the converter current, voltage and power for different solar irradiation scenarios. Source: Green PE project.*

The depicted lower currents are those flowing through the inductors for positive and negative halfwaves, respectively. Since switching occurs much quicker than the displayed resolution, the curves appear as solid areas. The achieved conversion efficiency is about 97%. This is better than commercially available products but is still not the full efficiency of this concept, as previous simulations have demonstrated. There is a need for further optimization to take the full advantage of the topology.

Any minor mismatches of the maximum power point lead to an immediate reduction of the overall efficiency, and they are quickly larger than those reductions in efficiency, introduced by converter hardware or topology itself. Therefore, accurate tracking of the MPP is an important issue and it has been spent much attention to adjust the apparent input impedance to the provided solar input power.

A record of the tracking performance is shown in Fig. 2.8, displayed as a characteristic curve for different solar irradiation scenarios.

On the left hand side is the curve for the input current shown and it becomes visible how the converter control tunes itself to a new operating point whenever an input current change is observed. This operating point is characterized by the maximized product of voltage and current, which is equivalent to the maximized power provided, as shown on the right hand side of Fig. 2.8.

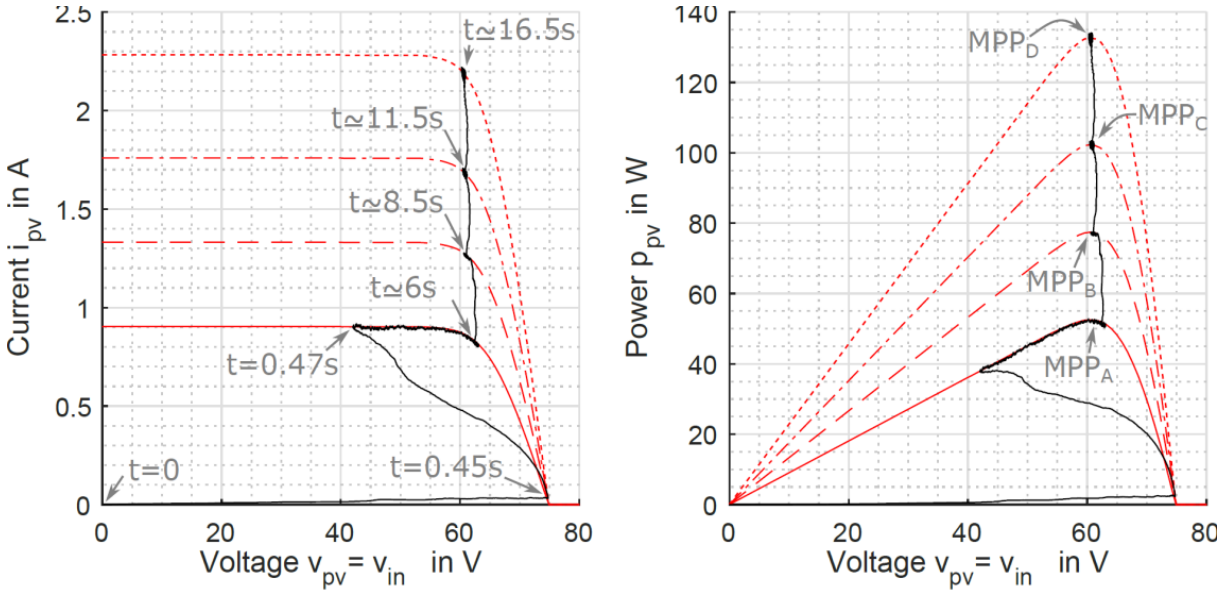


*Figure 2.8: Resulting, relative MPPT mismatch for the converter current, voltage and power for different solar irradiation scenarios. Source: Green PE project.*

## 2.6. Outcome of the fair activities: applications and market entry barriers

Beginning in 2016, different fairs and exhibitions have been visited, either by the Kiel University (CAU) itself or its associated partners within the project. Especially the PCIM Nuremberg (2016 – 2018), the WindEnergy Hamburg (2016), HUSUM Wind (2017), electronica Munich, Energy storage in Düsseldorf, and EES Europe in Munich were important in the field of renewable energy and have been used to present first the existing 1 MW power stack demonstrator at the early stage of the project and secondly the concept and realization of the DC/AC converter. Besides the solar application of the converter with its high efficiency in light load conditions, **additional applications** (and possible markets) have been discussed and identified as an outcome:

- Decentralized generation, distribution and conversion of electrical energy
- DC source: battery storage, subsea cable, DC line power supply in households
- High efficiency within a wide power range
- Passively cooled housing reduces need of maintenance and opens new fields of applications in harsh environments, such as automotive, construction vehicles, railroad auxiliary engines

The implemented innovations require for commercialization further development for specific applications and lead as a consequence directly to market entry barriers.

These are related – as the most relevant obstacles - to the effort to implement a micro controlled converter including computing power, the design and fundamental knowledge in novel PE architecture in possible companies, as well as the costs of wide bandgap devices.
On the other hand, **two very positive developments** to overcome the market entry barriers are observed:

1.) The **3-level topology** as demonstrated here is preferable in UPS and solar inverters because of its high efficiency and costs of devices with lower breakdown voltage. There is a positive feedback and a strong interest in this topology by companies. Therefore, the entry barrier for this development seems to be overcome and the technology becomes state of the art [see 2].
2.) The **reduced internal losses** have as a side effect a direct impact to heat dissipation. The demonstrator A1 of this project had demonstrated its feasibility within a passive cooled package. This results for potential companies and future collaboration in:
   - a design without containing nor requiring an active cooling or a radiator block or any moving parts for heat dissipation,
   - an easier thermal design and a more robust packaging concept,
   - novel markets and applications in automotive, hybrid or electric drives, harsh environments, and finally
   - a substantial competitive advantage on the market.

## 2.7. Outcome of the pilot demonstrator and future work

The pilot demonstrator shown here has proven its potential for a future exploitation in terms of efficiency, internal losses, modern topology and application of wide bandgap materials and advanced power density of remarkable 2.5kW/l (volume). In detail, the demonstrator delivers answers that lead to the following statements:

- model-based control makes the solar inverter robust and flexible,
- ZVS enables extreme high efficiency power converters,
- continuous modulation of frequency, dead time and duty cycle enables a broad power range,
- at such efficiency, MPPT must be given substantial attention,
- microcontrollers have sufficient computing power for a ZVS SiC Inverter.

In addition, at least three further activities are required to exploit the proposed advantages of the concept.

1.) There is still a gap of two percent in efficiency between the results shown in simulations compared to those achieved in lab tests. A further optimization of the control software will help to overcome this gap.
2.) As an extension, a 3-phase-setup seems to be the natural ongoing way of future work, as it fits at on hand to the requirements of some applications. Secondly, the power distribution in a 3-phase-setup is intrinsically balanced between the three lines and does therefore not require additional space consuming capacitors for a temporary storage of halfwave energy.

3.) For the pilot demonstrator, an external field test under real test conditions appears preferable. This would serve as an authoritative source for a data sheet of the demonstrator and pave the way to further collaborations and an accelerated time to market.
As a next step, it is planned to send the demonstrator to the University of Tartu to address the third point above. University of Tartu has at its facility the opportunity for a field test under real conditions including a competitive comparison to commercially available converter products. This will help to improve the device performance, the device readiness and open the way to oncoming collaborations.

## 3. A GaN-based inverter in Warsaw, Poland

The main goal of the GaN demonstration pilot was to show the performance of new transistors in a typical low-power single-phase DC/AC power converter, which is a common choice in the renewable energies application sector. Specific gains were expected by the reduction of the dimensions and weight due to the increase of switching frequency. At first, the decrease of the size and weight of the LC output filer was possible, then, application of the active power buffer was also investigated to reduce the necessary DC side capacitance. Moreover, a better long-term stability of the power converter parameters was expected due to the elimination of electrolytic capacitors.
Thus, the following research questions were asked:

- What is the performance of the system with reduced LC filter and transistors operating at 100 kHz?
- Are GaN transistors suitable to operate in active power buffers at switching frequencies up to 750 kHz?
- What are the features of the H-bridge inverter with an active power buffer operating at high switching frequency compared to a solution with electrolytic capacitors?
- Are new GaN transistors capable to operate at high switching frequencies?

A series of simulations & experiments were performed with high-frequency 2kV GaN H-bridge inverters, including operation with an active power buffer. Basically, all questions received positive answers. The obtained results show a correct operation of the GaN transistors in the main bridge with switching frequency of 100 kHz and, moreover, the obtained quality of the output waveforms with reduced LC filter is more than acceptable. The same transistors were tested at high switching frequencies operating with triangular current mode and zero current switching. The recorded waveforms confirm the correct operation of the active power buffer as power pulsations observed on the DC side of the inverter are decreased. All in all, the 2 kW inverter has shown very good performance with seriously reduced weight & dimensions (more details in the following chapters). At the same time, two key issues have been observed: The importance of the capacitors in the energy buffer (due to limitations of currently available technology) and the performance of the high-frequency control system of the active power buffer.

## 3.1. Technical introduction

Most common power conversion schemes applied in low-power renewable energy systems such as photovoltaics (Fig. 3.1a) or small wind turbines (Fig. 3.1b) use DC-AC inverters. This power electronic system converts DC voltage into AC voltage required to supply AC loads or feed energy to the distribution electrical grid. A popular topology applied in a single-phase DC-AC inverter is a H-bridge investigated in the pilot demonstrator.

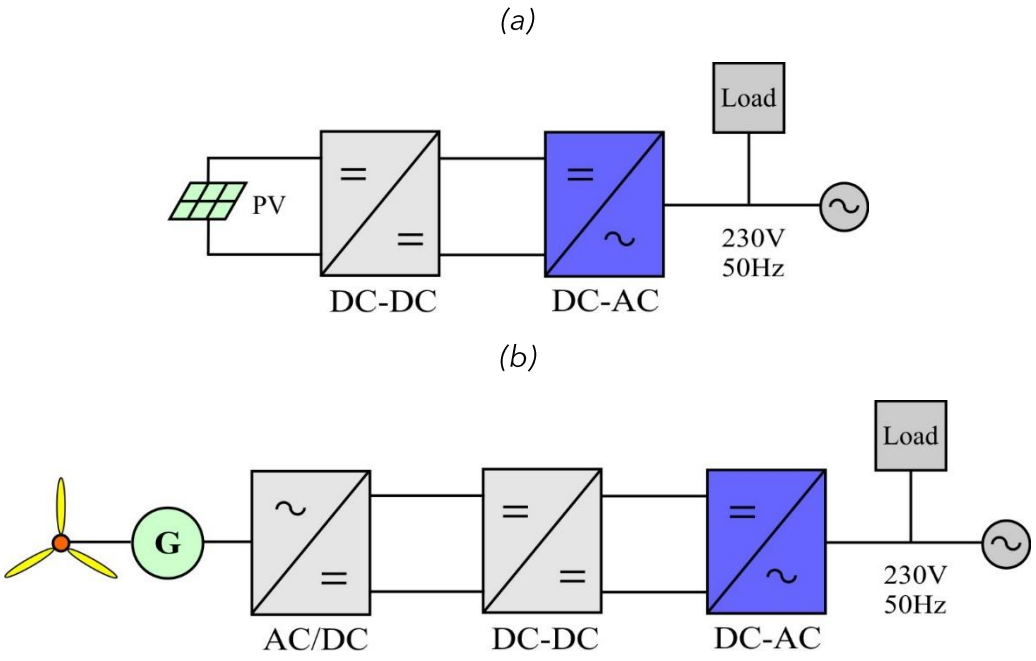


*Figure 3.9: Typical power conversion stages for renewable energies: a) photovoltaics, b) small wind turbines. Source: Green PE project*

## 3.2. Gallium nitride (GaN) technology

Due to better material features the Gallium Nitride transistors offer a number of advantages over their state-of-the-art Silicon counterparts but the main gain, from a power electronics point of view, is the better Figure of Merit calculated by multiplication of the on-state resistance and drain-source capacitance or gate charge. In practice, GaN transistors (majority are High Electron Mobility Transistors – HEMTs – see example in Fig. 3.2) operating in power converter circuits are faster, which lead to lower switching energies. A comparison of the gate charge characteristics of GaN HEMTs, SiC MOSFETs and Si superjunction MOSFETs (Fig.3.3) shows that less charge is required to turn-on/off GaN transistors. In other words, switching times can be shorter. Shorter switching times and lower amount of dissipated energies can be translated into much higher switching frequencies. As a consequence, size and weight of passive components may be decreased due to new, better transistors.

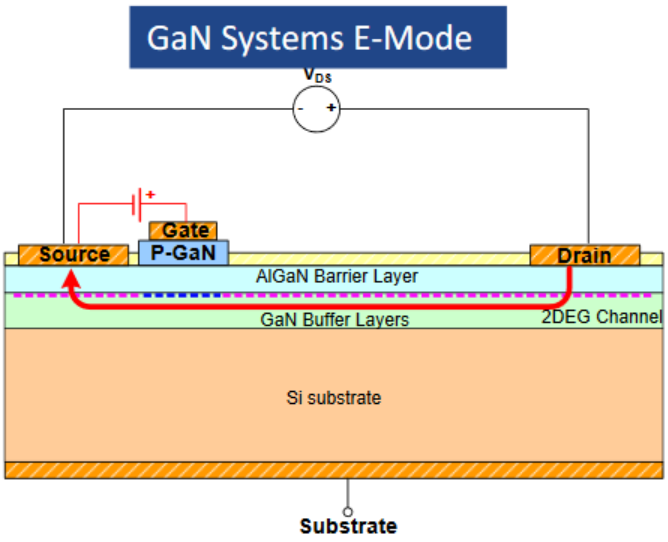


*Figure 3.10: High electric field & high electron mobility transistor structure.*
*Source: GaN Systems.*

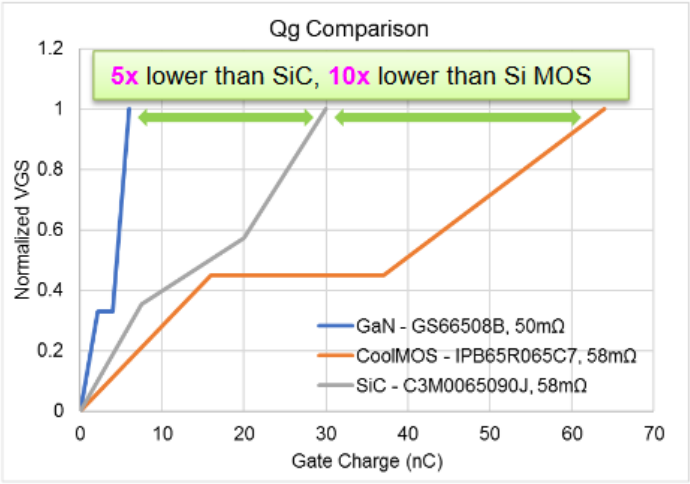


*Figure 3.11: GaN HEMTs parameters versus Si and SiC technology.*
*Source: GaN Systems.*

An analysis of currently available devices show that GaN HEMTs offer:

- Lower gate charges @ comparable on-state resistance
- Faster switching = higher frequencies & lower losses
- Blocking voltages < 650V – ideal for single phase operation
- Slightly different concepts among manufacturers
- Power devices with integrated gate drivers available

Expected benefits of using GaN HEMTs:

- Faster switching = higher frequencies = reduced size of LC filter
- Lower on-state resistances = lower conduction losses = smaller cooling system
- In total: **higher efficiency and power density**

## 3.3. GaN HEMTs in H-bridge inverter

The new technology of power semiconductor devices may be applied in a single-phase DC-AC inverter in order to improve the performance of the system. At first, the switching frequency of the main bridge transistors may be elevated to decrease the size and weight of the output filter. Then, DC side capacitors may be replaced by an active power buffer based on GaN transistors.

### 3.3.1. Reduction of the output LC filter

The application of GaN transistors, instead their Si counterparts, in a H-bridge inverter (Fig 3.4) strongly affects size and weight of the passive elements. As the output filter resonance frequency is directly related to the switching frequency of the transistor, an increase of the switching frequency leads to smaller and lighter filters (lower inductance and capacitance required). For the 2 kW system considered in this pilot demonstrator the increase of the switching frequency to 100 kHz together with an unipolar PWM modulation, allows for a decrease of the output LC filter size ($L_f$=2x40μH, $C_f$=1μF). Thus, the use of new transistors increases the power density of the power converter.

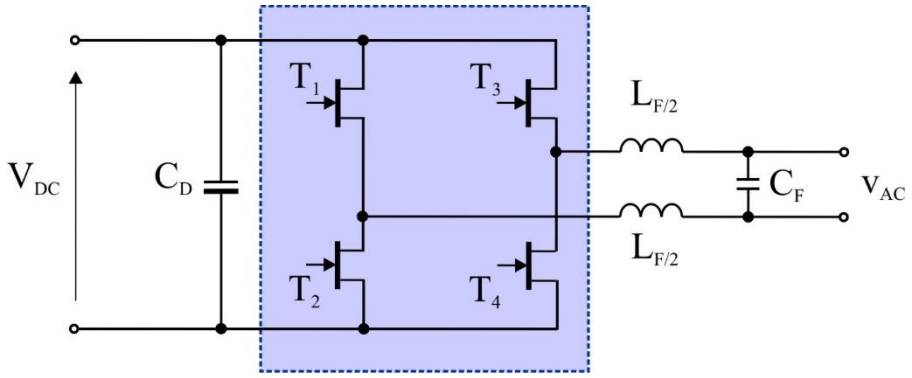


*Figure 3.12: H-bridge inverter topology based on GaN HEMTs.*
*Source: Green PE project.*

Demonstrator parameters:

- Nominal power 2kW
- Input voltage 400VDC
- Output voltage 230AC/50Hz
- Four transistors type GS66508T (650V/50mΩ)
- Gate driver: Si8274
- Inductor $L_F$=2x40μH
- Capacitor $C_F$= 1μF
- Switching frequencies may be increased above 100 kHz without serious efficiency decrease

The pilot demonstrator of the H-bridge inverter was designed with a top-cooled GaN HEMTs from GaN Systems. The PCB is presented in Fig. 3.5 where the suitable mounting method, enabling a good thermal performance and electrical connections, is visible.
In addition to the transistors, gate drivers and supplies, SMD capacitors of the DC side are visible.

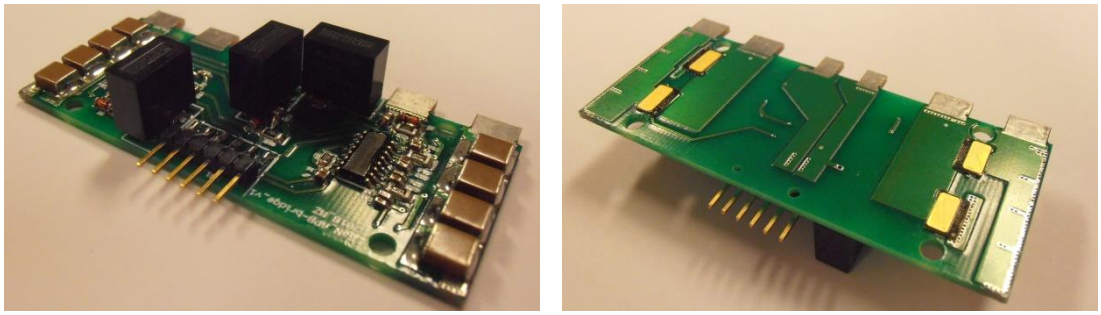

*Figure 3.5: Photo of the H-bridge demonstrator – top and bottom views.*
*Source: Green PE project*

The designed H-bridge inverter was controlled with an unipolar PWM modulation at 100 kHz in open-loop control and feed from a 400V DC supply. The waveforms of the output voltage and current recorded during laboratory tests at nominal conditions (2kVA) are presented in Fig. 3.6a. The high switching frequency enables good quality of the output waveforms even with a strongly reduced LC filter size. Moreover, the observations with a thermal camera also prove a good thermal performance of the inverter with the transistors mounted on the air-forced cooled heatsink.

*(a)* *(b)*

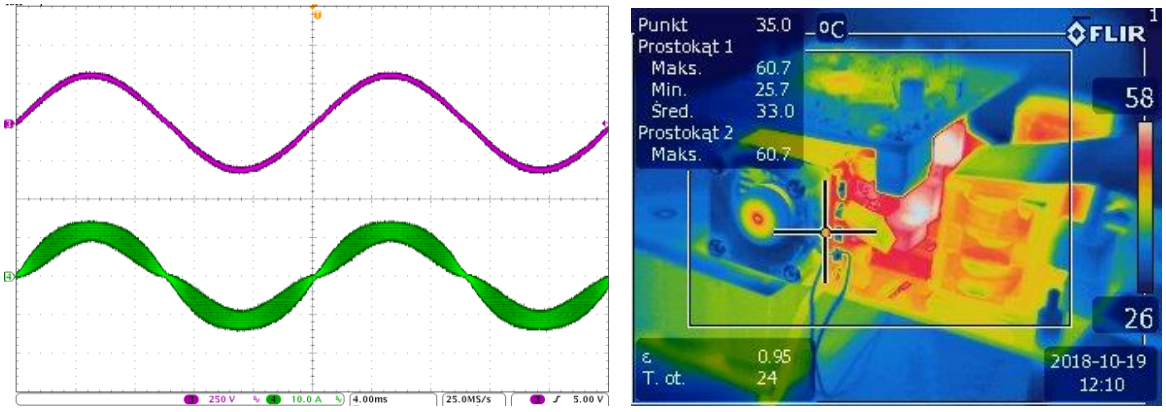


*Figure 3.6: Results from laboratory tests – AC voltage and AC current waveforms (a) and picture from thermal camera (b).*
*Source: Green PE project*

### 3.3.2. Active power buffer (APB) with GaN transistors

Unfortunately, the high switching frequency of the H-bridge transistors does not affect the size of the DC-side capacitor, aluminium electrolytic technology is usually applied here with all advantages (high capacitance per volume, low cost) and disadvantages (weak parameter stability, high losses). Therefore, the DC-side capacitor necessary to reduce low frequency pulsations, is a significant part of the converter when volume and weight are measured.

Very good performance of GaN transistors may be used to eliminate or reduce the DC-side capacitor by application of an active power buffer. This solution, known in the literature since a couple of years, introduces a fast DC-DC converter with capacitive energy storage to compensate low frequency power pulsation – see [3]. Two transistors of the DC-DC may be GaN HEMTs, which enable switching frequencies well above 100 kHz.

Furthermore, when a special control with turn-on at zero current is introduced this frequency may be higher than 500 kHz, which seriously limits the size of the necessary inductor to 40 µH. All in all, the active power buffer ensures good quality of the DC and AC waveforms with DC-side capacitor decreased to 15 µF only.

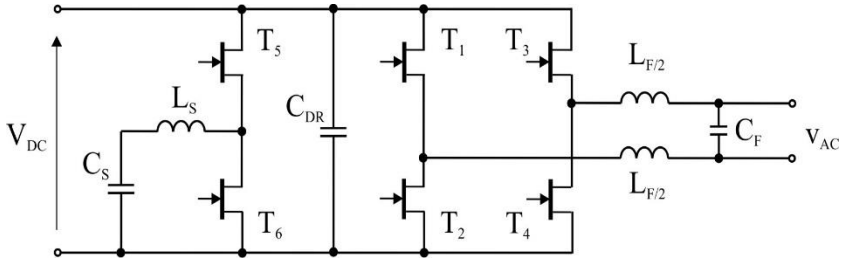


*Figure 3.7: H-bridge inverter topology with Active Power Buffer (APB).*
*Source: Green PE project*

The operation of the APB is based on tracking the pulsation of the power (see simulations in Fig.3.8). In order to limit the size of the DC capacitor the same power with negative sign has to be injected by the active power buffer. As a consequence, as power is pulsating at double load/grid frequency the voltage of the storage capacitor is charged and discharged with the same frequency.

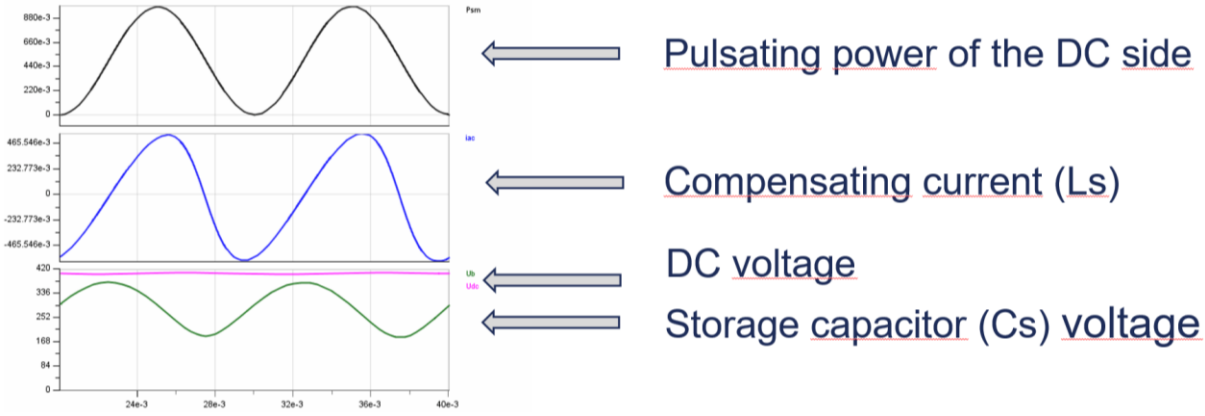


*Figure 3.8: Operation principles of Active Power Buffer (APB).*
*Source: Green PE project*

On the base of circuit simulations, the following parameters of the APB were determined:

- CS is related to compensated power, 120 µF is selected (Ceralink)
- LS = 40 µH, depends on switching frequency of T5/T6 and control method
- GaN HEMTs enables operation at hundreds kHz
- remaining DC capacitor – 12 x 2.2 µF (SMD) + 20 µF (ceralink)

As can be seen in Fig. 3.9 the PCB with two transistors and gate drivers was mounted on the second side of the heatsink. A view of the complete design H-bridge inverter with APB is presented in Fig. 3.10, powerboards are shown in Fig.3.11.
The final view of the 2 kW demonstrator is presented in Fig. 3.12 – dimensions of the model are 85mm x 160 mm x 50 mm (WxLxH). This leads to volume of 0,68 $dm^3$ and power density of 3 $kW/dm^3$.

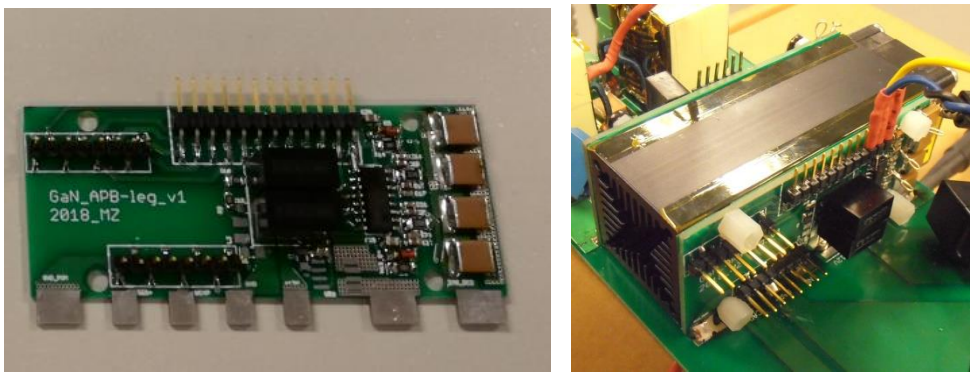


*Figure 3.9: Photo of APB demonstrator – PCB alone and mounted on the heatsink.*
*Source: Green PE project*

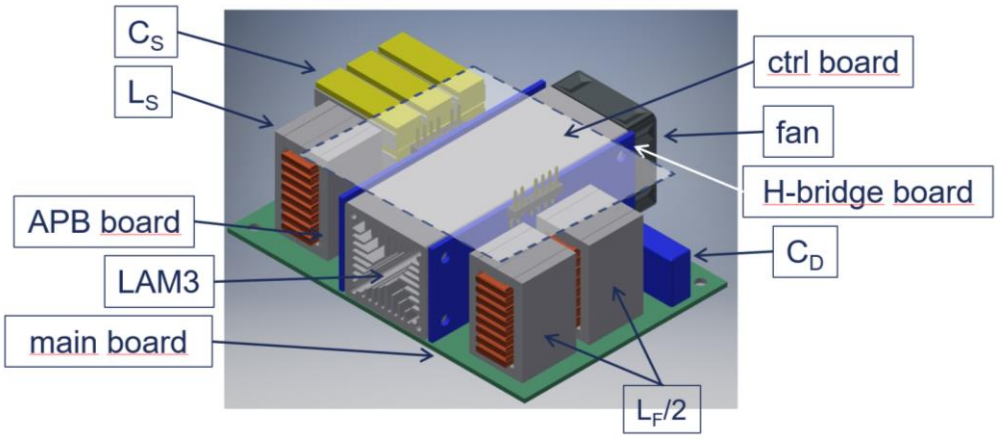


*Figure 3.10: 3D view of the main components.*
*Source: Green PE project*

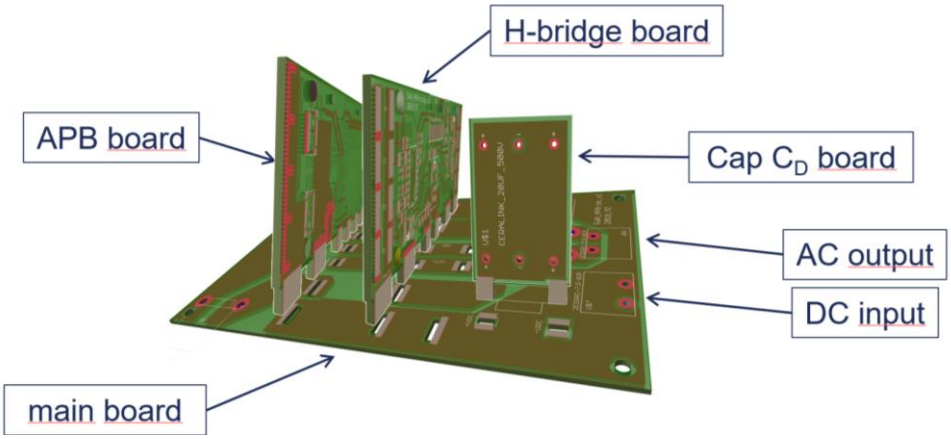


*Figure 3.11: 3D view of the powerboard.*
*Source: Green PE project*

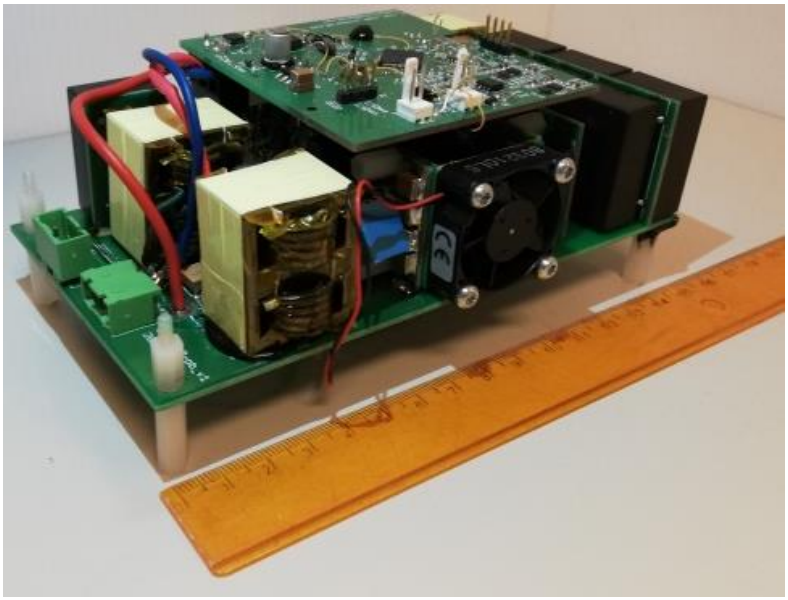

*Figure 3.12: Picture of the prototype.*
*Source: Green PE project*

## 3.4. Active power buffer – control algorithm

Control algorithm of the APB is challenging [3], [4], especially when high frequency operation (> 100 kHz) is taken into account. On the base of literature and simulation studies the control algorithm of the H-bridge inverter with APB was developed. It consists of three main parts:

- Startup procedure
- Output power management
- APB control

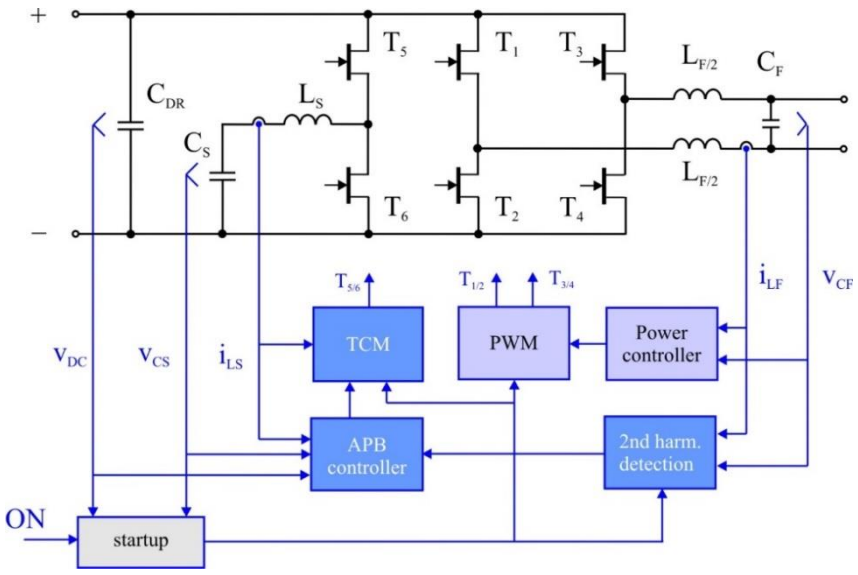


*Figure 3.13: Diagram of control algorithm of H-bridge inverter with APB.*
*Source: Green PE project*

### 3.4.1. Start-up procedure

It is obvious that correct operation of the inverter and, especially, active power buffer, requires defined initial conditions. For sure, the storage capacitor has to be initially charged before APB starts any compensation. Therefore, a start-up procedure has been developed and tested during simulations – see results in Fig. 3.14. After applying the DC voltage, the APB transistors are controlled to draw constant current from the input voltage source and charge the storage capacitor to 280V. According to performed simulations this process takes around 6ms and, after 10ms (half period of the 50 Hz grid) the inverter is ready to operate.

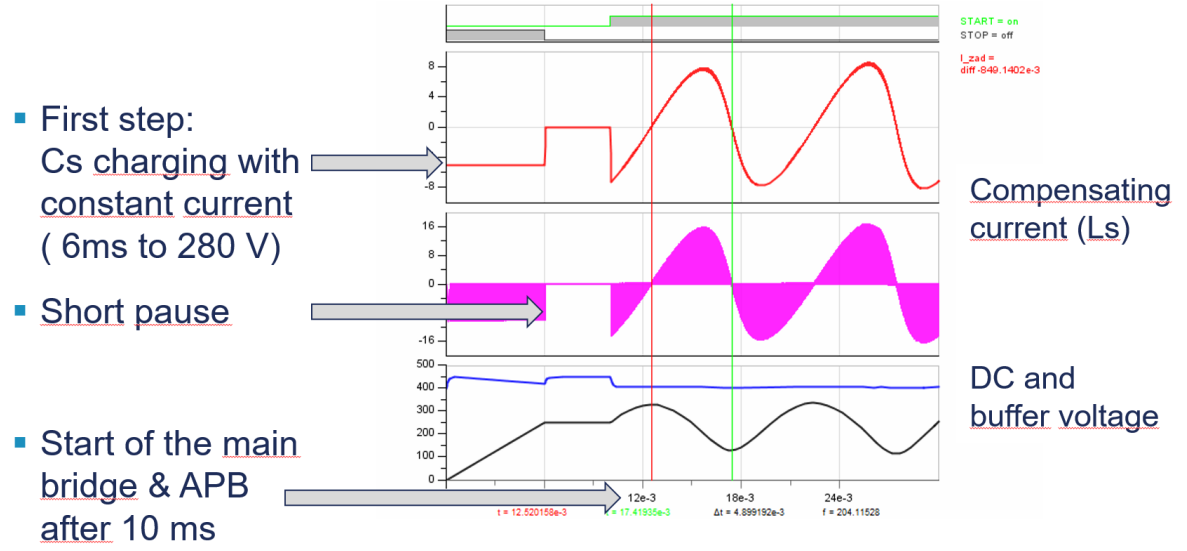


*Figure 3.14: Start-up procedure of the APB – simulation results.*
*Source: Green PE project*

### 3.4.2. Output power management

Usually, each DC-AC inverter requires output power management to process the required power – supply the grid or AC loads. In the presented case a proportional-resonant (PR) controller of the output current is applied – this is a very common solution in such inverters. The simulations presented in Fig. 3.15 show the start of the inverter at the nominal load – as can be seen, the PR controller reduces errors during a single 20ms period. Moreover, the tested system (including active APB) is able to operate during step changes of the output power – see Fig.3.16.

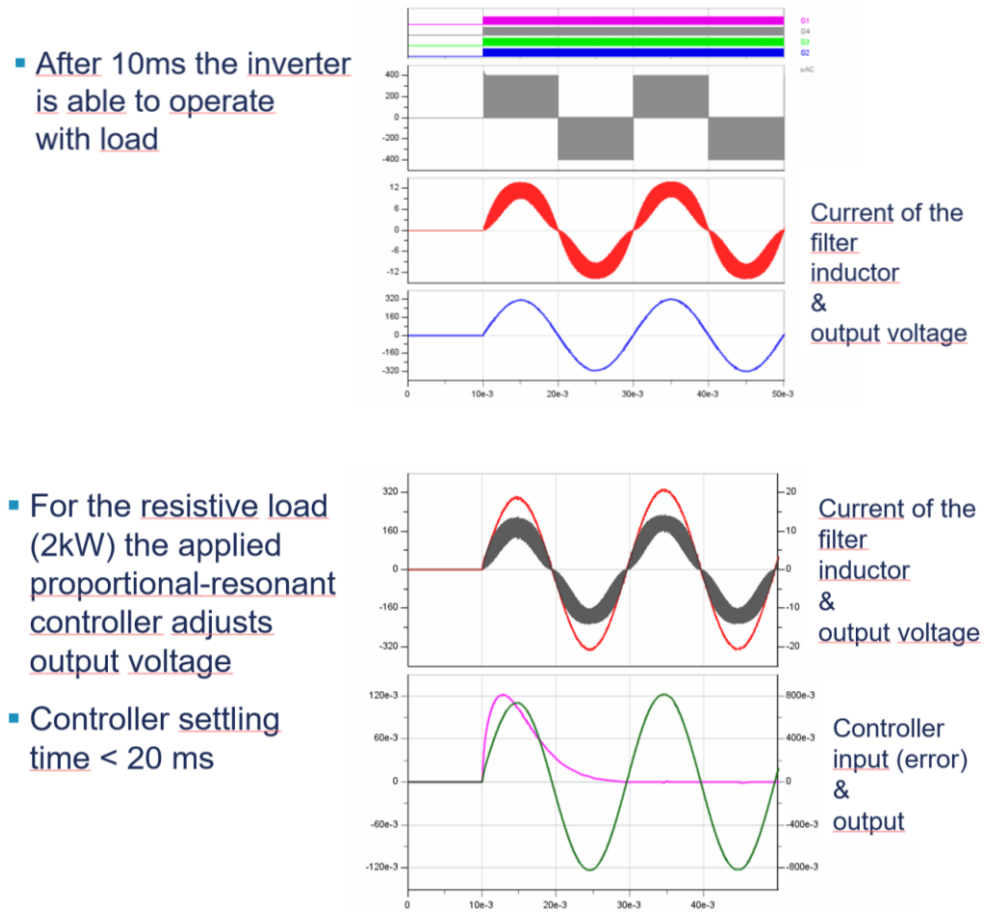


*Figure 3.15: Simulation results presenting power management.*
*Source: Green PE project*

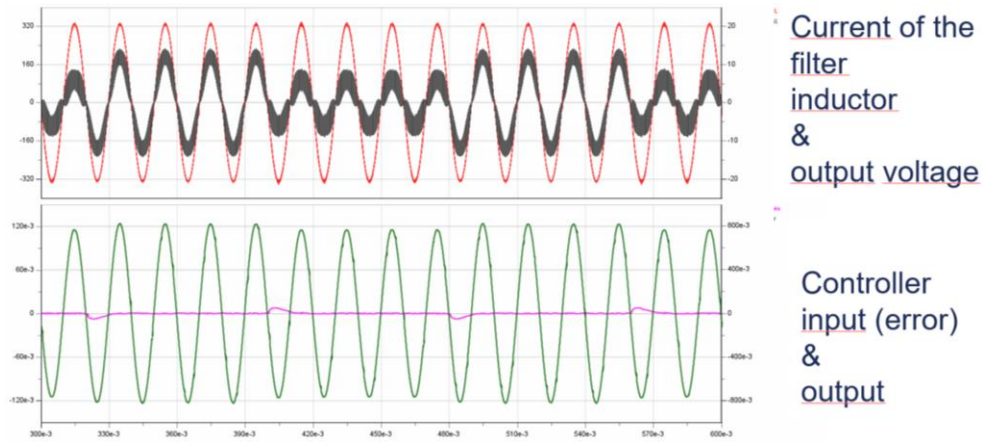


*Figure 3.16: Simulation results presenting power management: step changes of the load power (2kW/1kW).*
*Source: Green PE project*

### 3.4.3. APB control

The definitely most complex part of the control algorithm is the one related to APB – see scheme in Fig. 3.17. Three major functions may be distinguished:

- Detection of the pulsating power – based on output voltage and current measurements and low-pass filtering,
- DC component of the storage voltage managed by PI controller
- Constant current charging at start

  The current of the storage is adjusted by suitable switching of T5/T6 according to the Triangular Current Modulation (TCM) [4]. This method provides zero current switching (ZCS) and is characterized by a variable switching frequency.

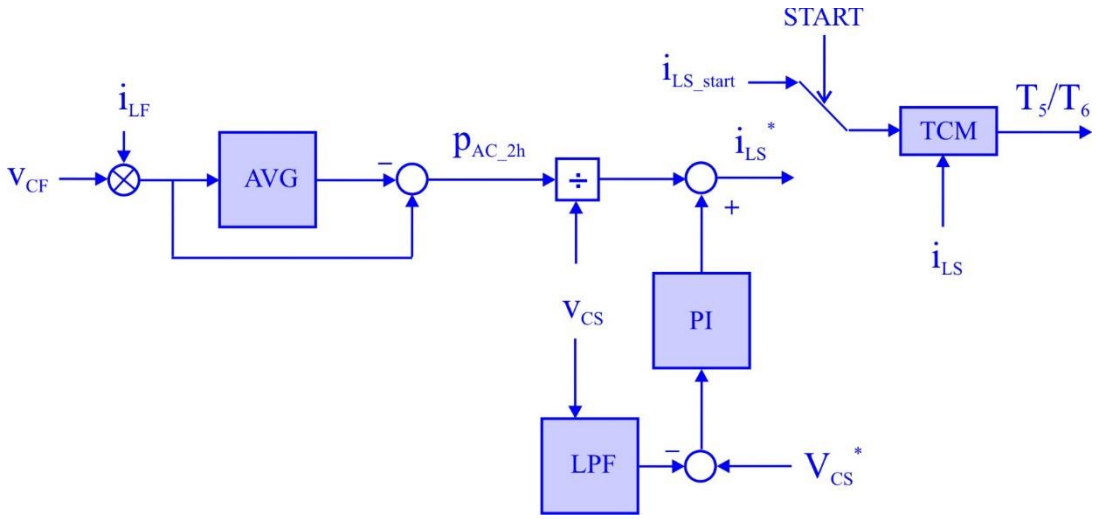


*Figure 3.17: Control algorithm of the APB (with TCM).*
*Source: Green PE project.*

The control algorithm of the APB was simulated to verify the whole concept. At first, the start of the APB operation is presented in Fig.3.18 – it is shown that after 100 ms the PI controller of the DC component reaches steady-state conditions and the voltage of the storage capacitor is oscillating around the reference value. The next presented test is the operation of the APB during step changes of the output power (see also Fig. 3.16). The implemented algorithm follows step changes of the output power to compensate DC voltage pulsations.

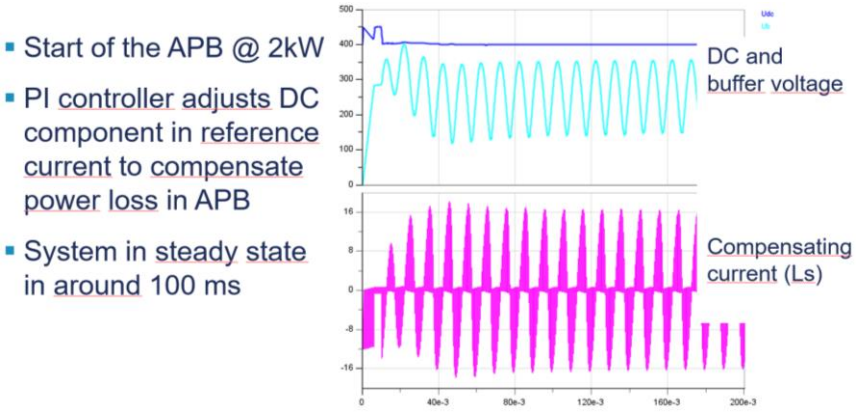


*Figure 3.18: Control algorithm – APB: PI controller (Ucs) – simulation results.*
*Source: Green PE project*

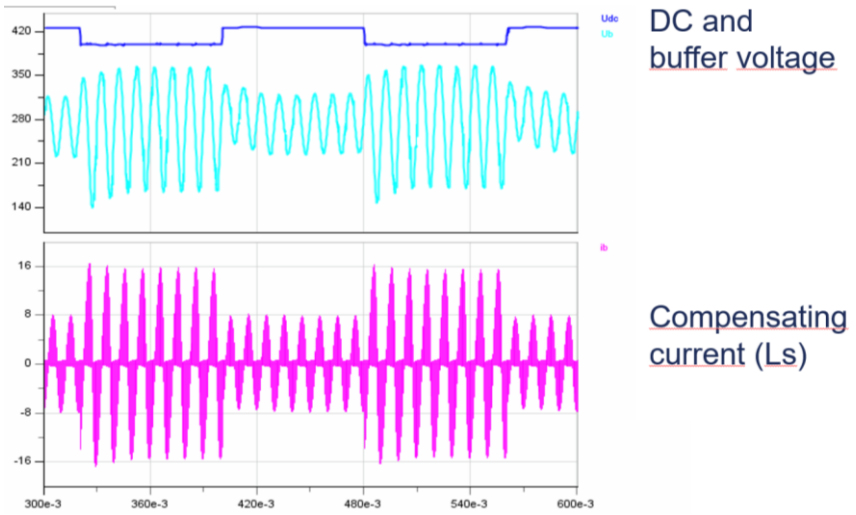


*Figure 3.19: Control algorithm – APB: PI controller (Ucs): step changes of the load power (2kW/1kW).*
*Source: Green PE project*

## 3.5. Demonstrator of the GaN H-bridge inverter with APB

### 3.5.1. Power stage

A scheme of the power section of the H-bride inverter with APB is presented in Fig. 3.20. In addition to the two inverter legs with GaN HEMTs, equipped with gate drivers, another leg, which serves as an APB, is also introduced. Suitable sensors, necessary to implement the discussed control algorithm, are applied. Finally, supply voltages for all components are provided. Photos of the designed PCBs are presented in Fig. 3.5 and 3.9.

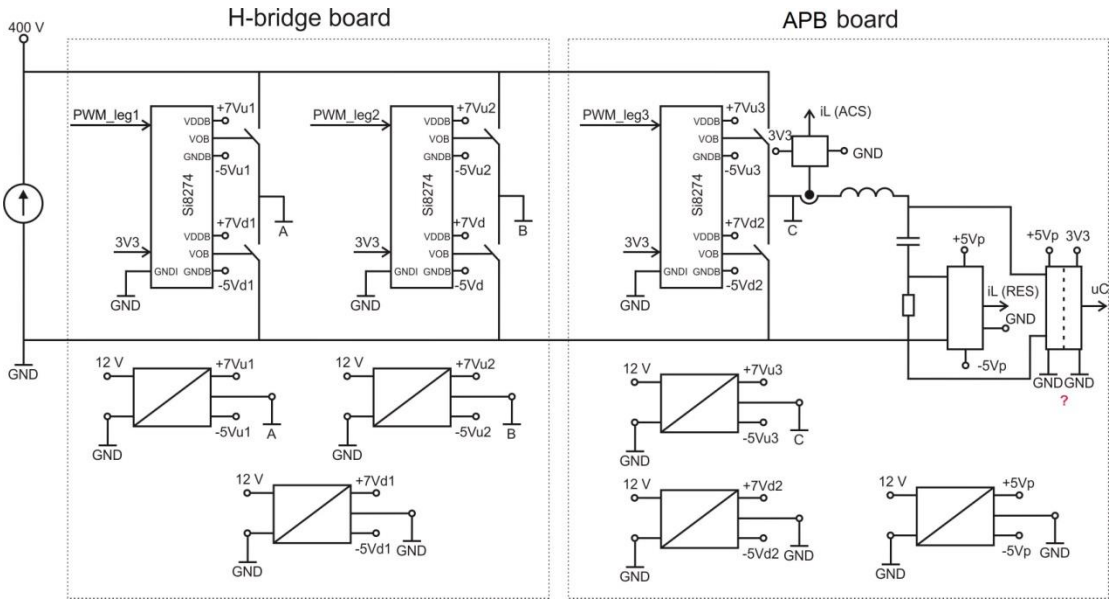


*Figure 3.20: Detailed block scheme of power circuit.*
*Source: Green PE project*

## 3.5.2. Control stage

A control stage of the inverter is slit to two blocks as shown in Fig. 3.21. The first is the digital control module responsible for PWM signal generation for the main output H bridge, output current and voltage measurements, generating a control reference signal for the APB control circuitry module and handling additional peripheral devices such as fan control and user interface. The detailed functional diagram of this block is shown in Fig. 3.22. The main processing unit of this block is a Cortex-M4+ based CPU (STMicroelectronics STM32F405RGT7). The main task for this module is generating proper PWM signals to the main H-bridge and performing output parameters measurements. The module is powered from internal 12 V DCC of the inverter and it is equipped with its own power block generating proper voltages for operation. One of the most important submodules is a fully isolated output measurement block providing output voltage and current. This information is used for the digital implementation of the "WPM" and "Power controller" blocks shown in Fig. 3.13. The digital control module allows driving APB control circuitry in two modes. The user can choose either direct APB control from the digital controller through direct PWM signal generation or indirect control if the APB control module is present.

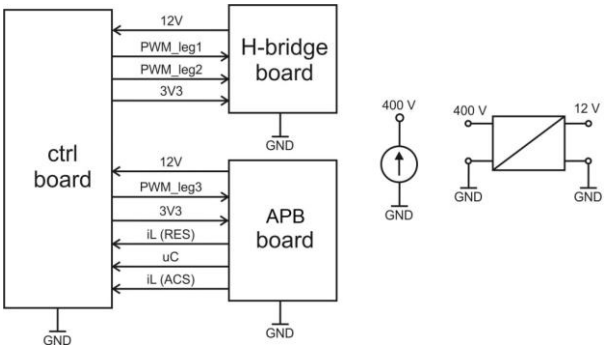


*Figure 3.21: Detailed block scheme & signal flow.*
*Source: Green PE project*

In the latter case, this module performs a digital detection of the 2nd harmonics and provides a reference signal for the APB controller block through driving fast DAC peripherals localized on the APB control board and other digital signals needed for the APB circuitry for proper operation. Fig. 3.23 shows the layout and photo of the digital control board. In this mode full triangular modulation is implemented as described earlier. In both direct and indirect driving modes, the module is also capable of measuring APB Cs capacitor currents.

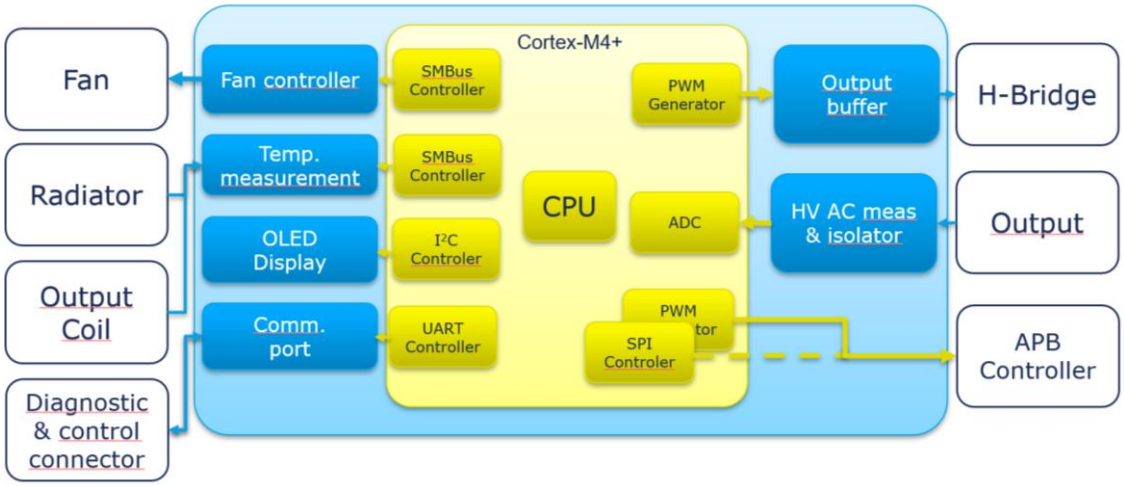


*Figure 3.22: Block diagram of control module.*
*Source: Green PE project*

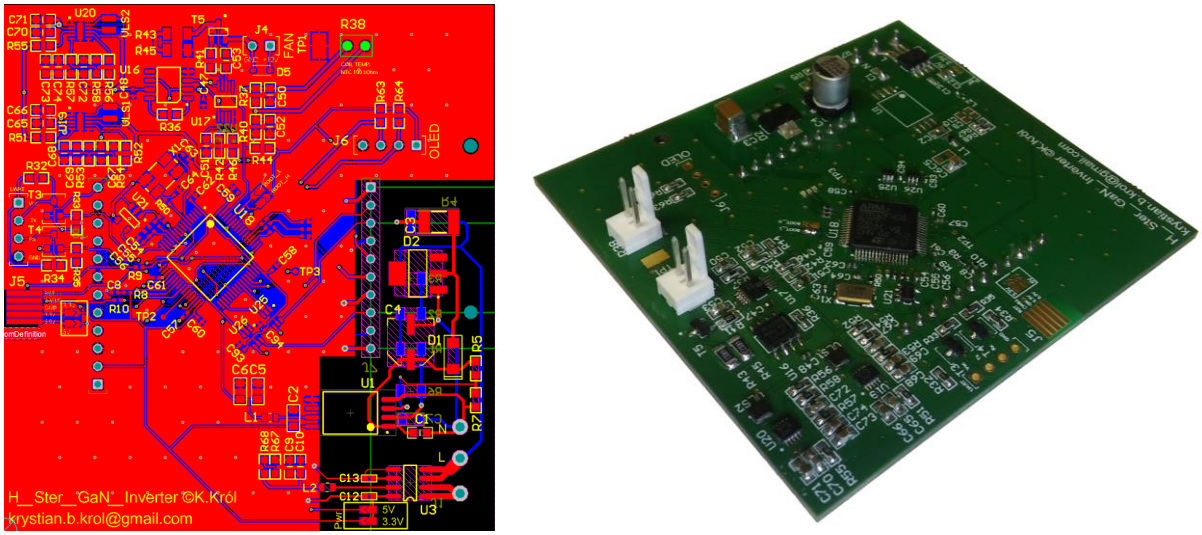


*Figure 3.23: Layout of control PCB and photo of prototype.*
*Source: Green PE project*

Since a fast operation of the APB control circuitry is required especially for high DC voltages this control stage was realized almost entirely analogue. The block diagram of the implementation of control algorithm shown in Fig. 3.17 is shown in Fig. 3.24. The only digital part of the device is a fast DAC converter providing reference voltage for the TRM method based on the 2nd harmonics calculations made in the digital control block. The main channel of the APB control block has wide band with unity gain frequency of at least 10 MHz allowing operation of the TRM modulator with frequencies up to 0.8-1 MHz without introducing nonlinear distortions. The APB control block is designed to be mounted at the back side of the inverter directly above the APB power stage. The design layout and 3D CAD model is shown in Fig. 3.25. Fig 3.26 shows the mounted APB control block during parameter measurements.

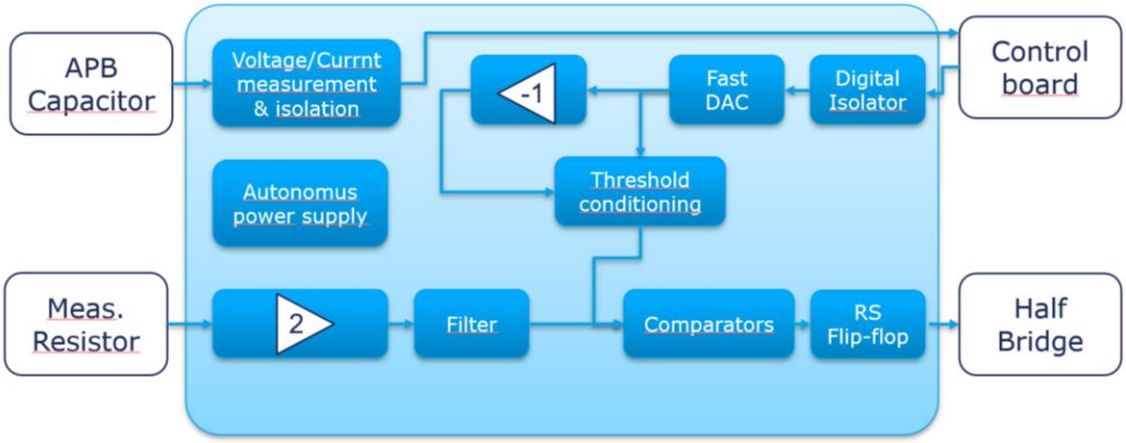


*Figure 3.24: Block diagram of APB controller.*
*Source: Green PE project*

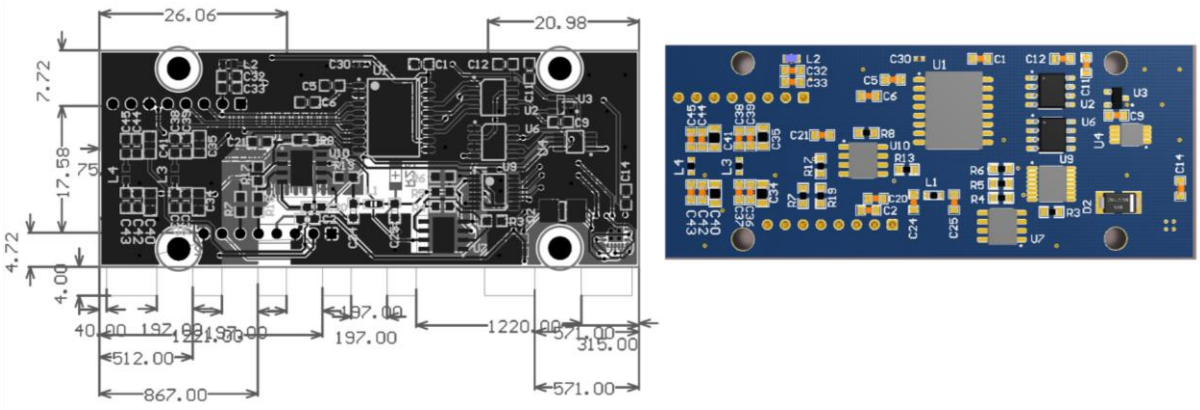


*Figure 3.25: Layout of APB controller and 3D CAD model of PCB prototype.*
*Source: Green PE project*

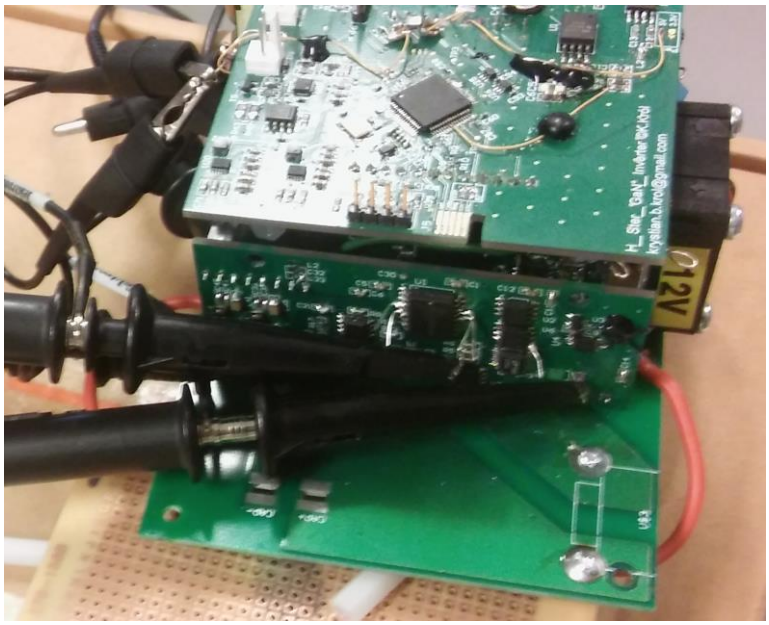


*Figure 3.26: Mounted APB control block during initial measurements.*
*Source: Green PE project*

## 3.6. Laboratory tests

The 2kW demonstrator of the H-bridge with APB was tested in a circuit as presented in Fig. 3.27. The whole system was supplied from a regulated DC supply with series resistors to emulate the behaviour of the PV panels, especially the DC voltage at the input of the inverter is pulsating due to this resistor.

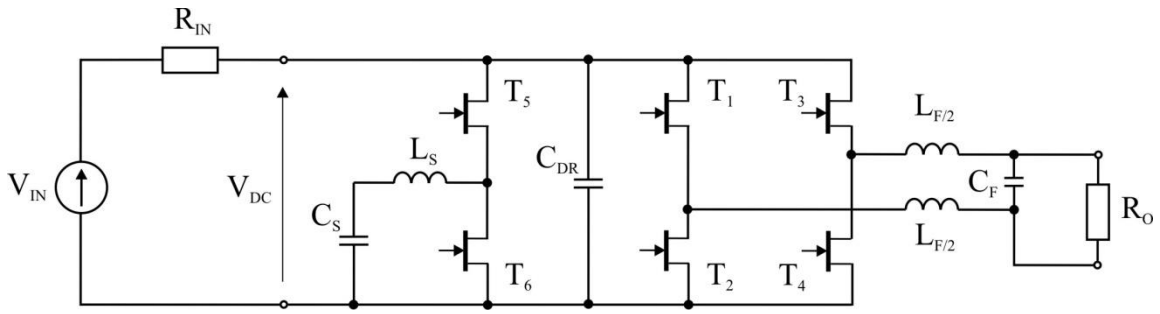


Figure 3.27: Scheme of the test setup.
Source: Green PE project

The measurements were focused on the APB operation. Fig. 3.28 shows a start of the APB, while the system was operating with inactive APB and pulsations of the DC voltage were not compensated (peak to peak voltage around 20V). After start of the APB, this pulsation is reduced around a factor of 4. According to the previously presented simulations, the pulsations should be even more reduced but, in practice, a number of additional factors (i.e. measurement delays) influences the final results. All in all, the pulsations of the DC voltage are kept at an acceptable level after an activation of the APB. Fig. 3.29 shows the current of the inductor in APB. It is clearly visible that the switching frequency is changing according to TCM rules and is counted in hundreds of kHz.

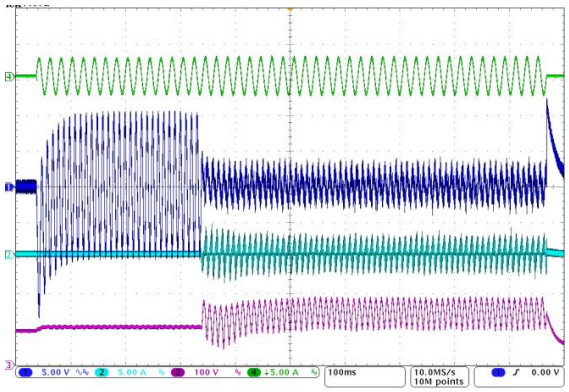

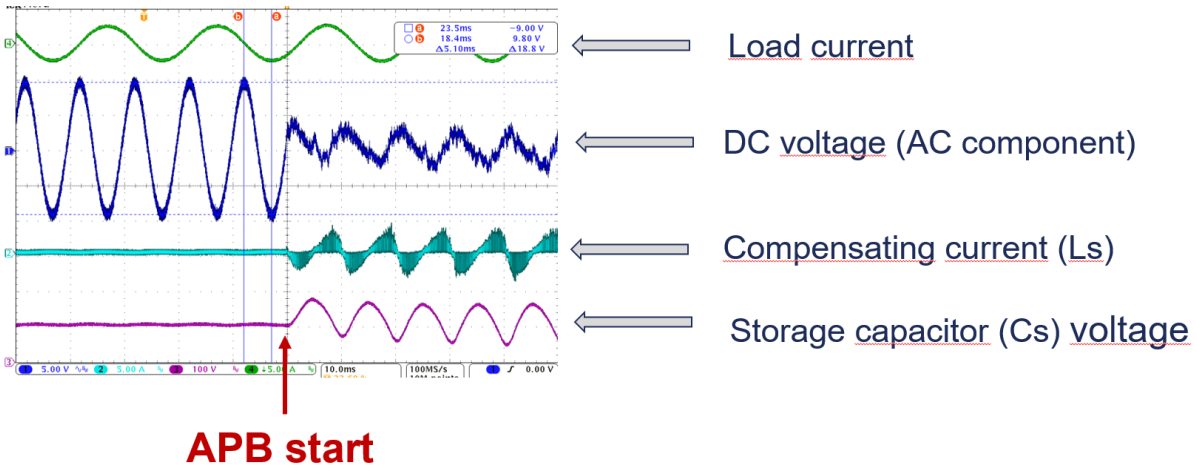


*Figure 3.28: Active Power Buffer operation.*

*Source: Green PE project*

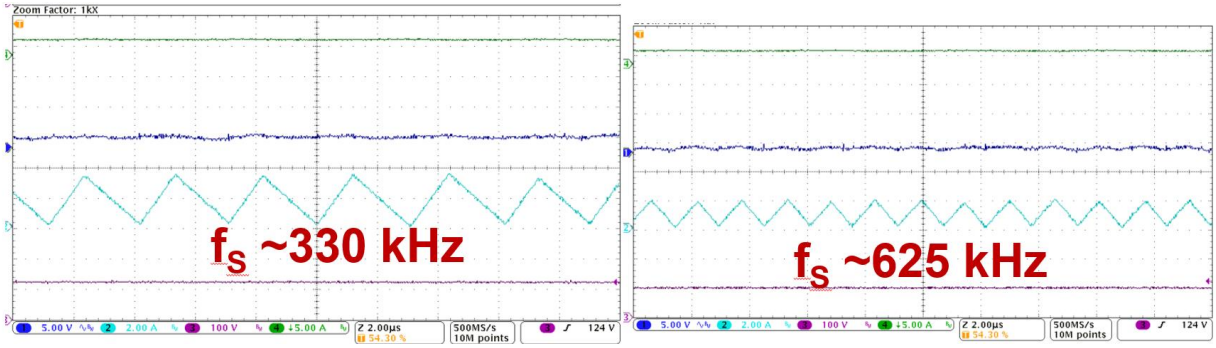


*Figure 3.29: Active Power Buffer steady state operation with variable frequency.*

*Source: Green PE project*

## 3.7. Summary

The performed analysis, simulations, and experiments on the demonstrator lead to the following basic conclusions:

- GaN HEMTs show great potential in the area of renewable energies
- Inverters may be smaller & lighter by implementing new transistors
- The LC filter size is reduced due to the increased switching frequency
- Bulky DC capacitors may be replaced by active power buffers
- The Size of the APB is comparable to a capacitor bank due the high switching frequency of GaN HEMTs
- The volume of the designed inverter is 0.68 $dm^3$ while a power density of 3 $kW/dm^3$ was obtained

## 4. List of Literature

[1] (Yu 2016) Z. Yu, H. Kapels and K. F. Hoffmann - A Novel Control Concept for High-Efficiency Power Conversion with the Bidirectional Non-inverting Buck-Boost Converter, EPE'16 ECCE Europe, Karlsruhe, 2016.

[2] Yole Developpement, 2018. Report - Status of the Power Electronics Industry 2018, September 2018, pp.131-132

[3] R. Wang et all, A High Power Density Single-Phase PWM Rectifier With Active Ripple Energy Storage, IEEE Trans. On Power Electronics, No. 5, May 2011

[4] D. Neumayr et all, Ultra-Compact Power Pulsation Buffer for Single-Phase DC/AC Converter Systems, Proc. Of IPEMC-ECCE Asia 2016.

# APPENDICES

Schematics about the pilot demonstrator A2

*Power board layout*

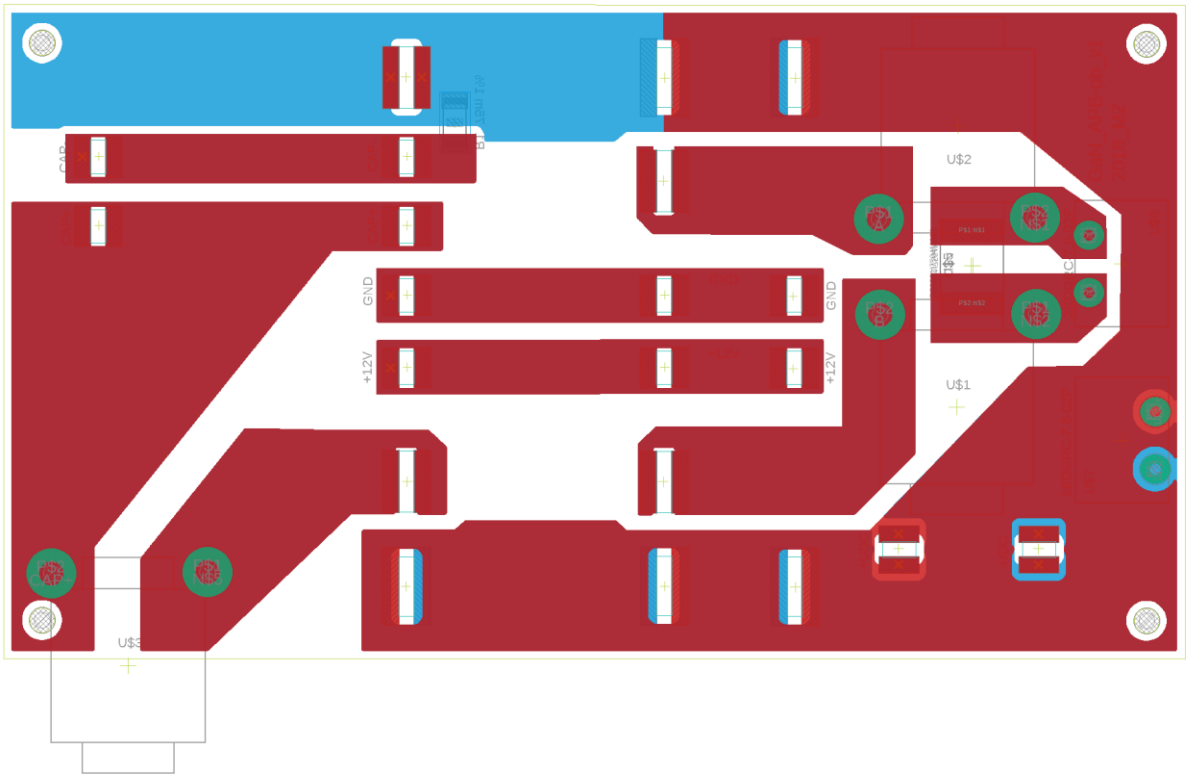


*Capacitor bank schematic for APB*

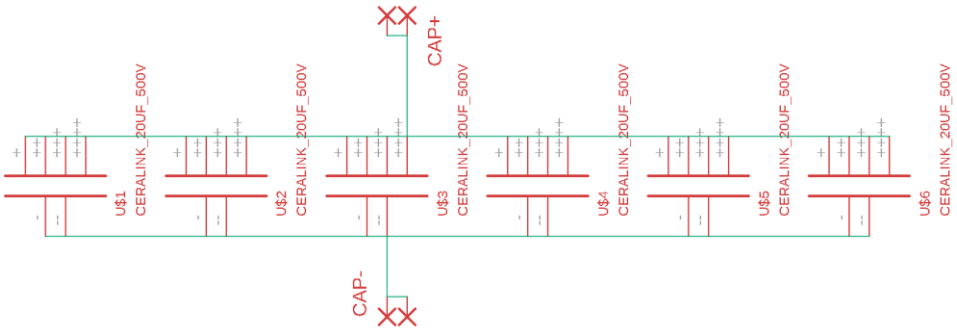


*Capacitor bank for APB (board layout)*

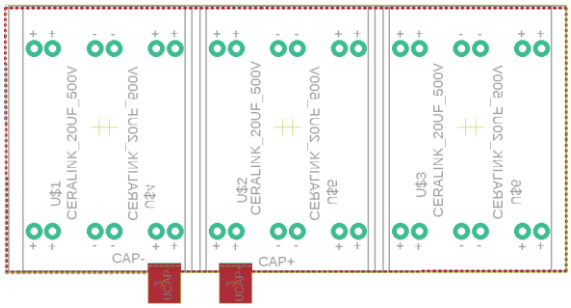

*H-bridge schematic*

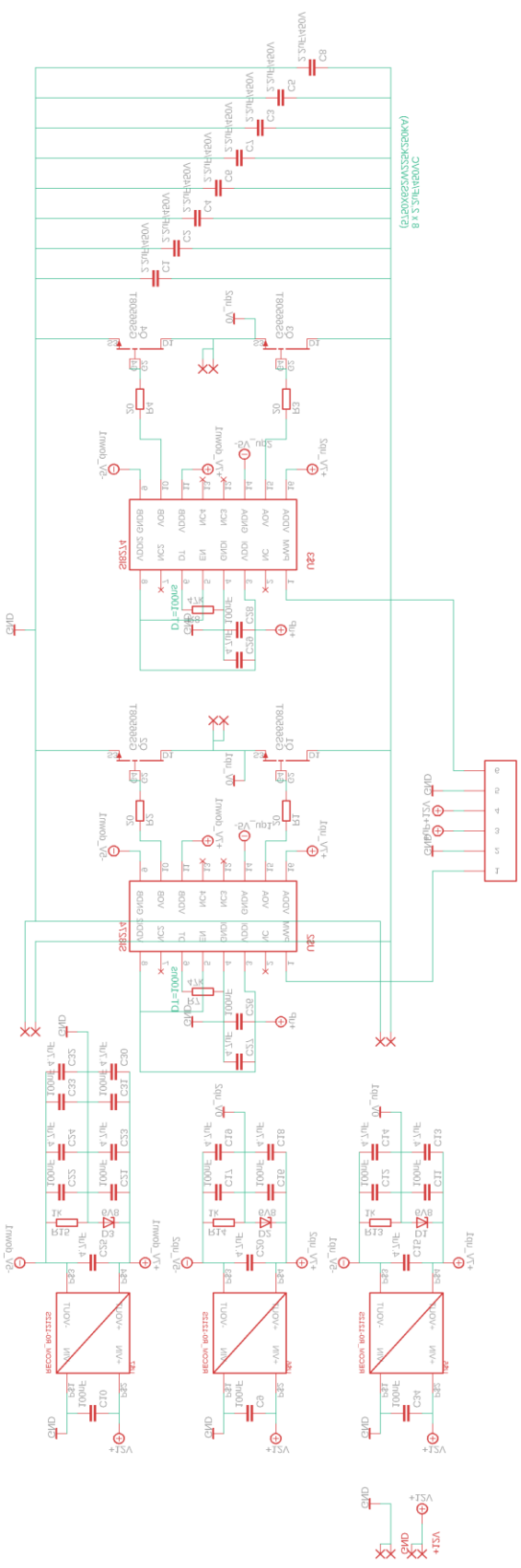

*APB-leg schematic*

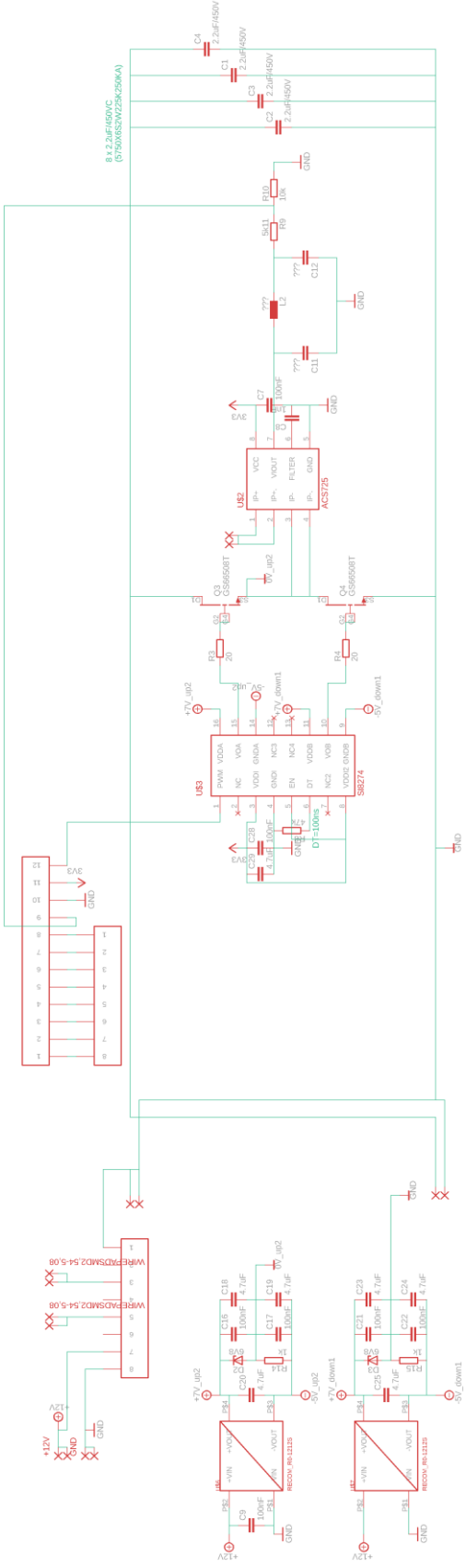

*H-bridge board layout*

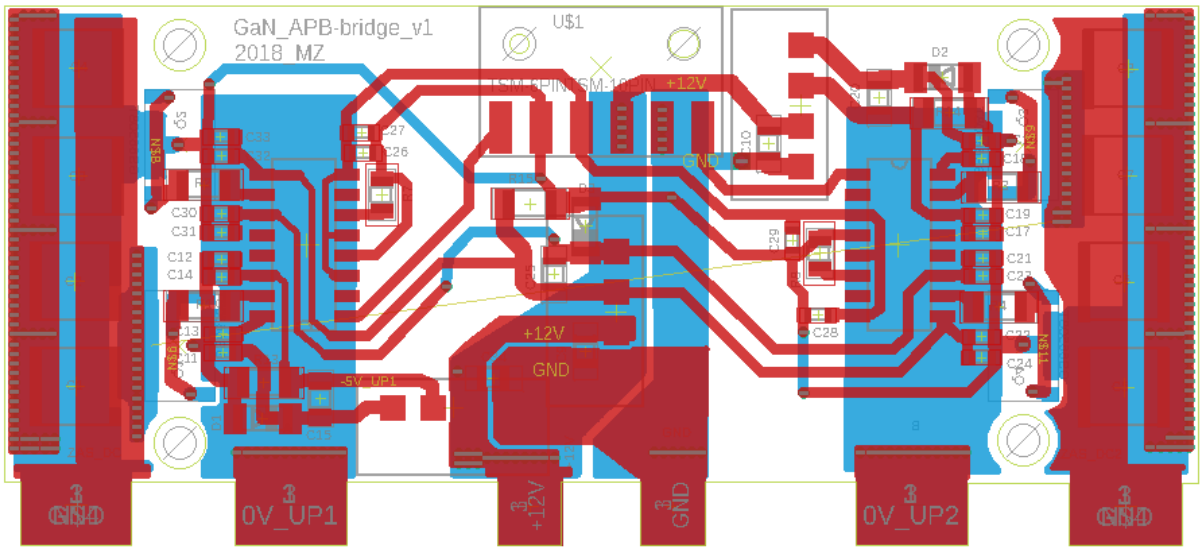


*APB board layout*

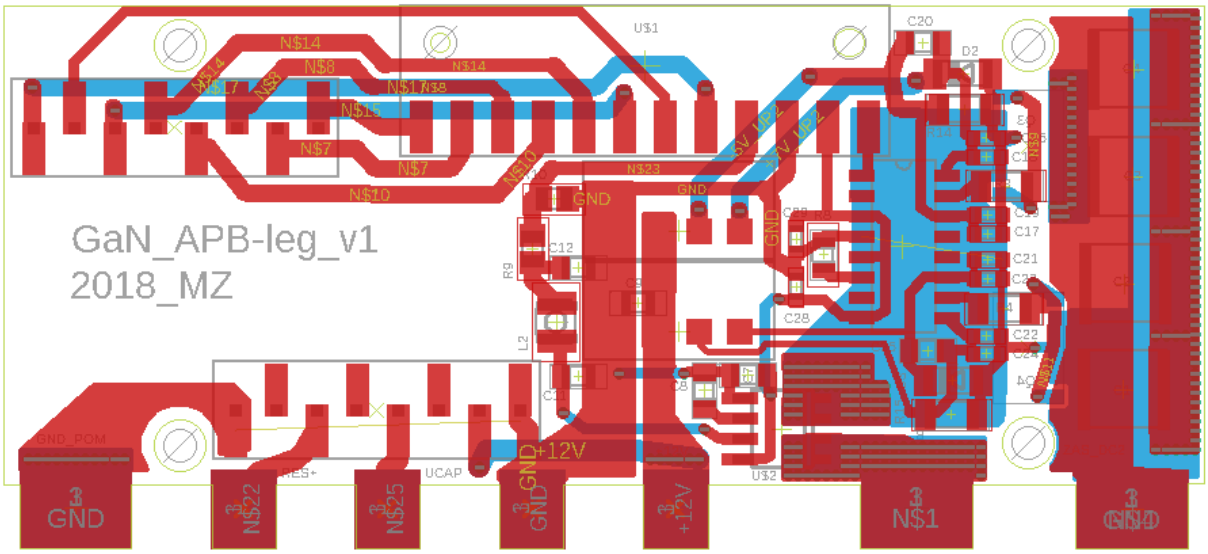

## Project Facts

- 17 project partners: research institutions, companies and technology transfer organisations
- Duration from 2016 to 2019
- Budget: EUR 3.1 mllion
- European Regional Development Fund
- Interreg Baltic Sea Region Programme
- Led by University of Southern Denmark

## Project Partners

- University of Southern Denmark (Denmark)
- Applied Research Institute for Prospective Technologies (Lithuania)
- Christian Albrechts Universität Kiel (Germany)
- CLEAN (Denmark)
- Converdan A/S (Denmark)
- Kaunas Science and Technology Park (Lithuania)
- Kaunas University of Technology (Lithuania)
- Latvian Technological Center (Latvia)
- NATEK Power Systems AB (Sweden)
- Polish Chamber of Commerce for Electronics and Telecommunications (Poland)
- Renewable Energy Hamburg (Germany)
- RISE Research Institutes of Sweden AB (Sweden)
- Sustainable Smart Houses in Småland (Sweden)
- Ubik Solutions OÜ (Estonia)
- University of Latvia (Latvia)
- University of Tartu (Estonia)
- Warsaw University of Technology (Poland)

green power electronics
innovation via new materials

Interreg
Baltic Sea Region

EUROPEAN UNION
EUROPEAN REGIONAL DEVELOPMENT FUND